ACS APPLIED MATERIALS & INTERFACES

www.acsami.org

Research Article

Low Concentration DMF/H_2O Hybrid Electrolyte: A New Opportunity for Anode Materials in Aqueous Potassium-Ion Batteries

Xinran Yuan, Yibo Li, Yanan Zhu, Wenjun Deng, Chang Li, Zhuqing Zhou, Jun Hu, Man Zhang, Haibiao Chen, and Rui Li*

Cite This: https://doi.org/10.1021/acsami.1c08151

Read Online

ACCESS | Metrics & More | Article Recommendations | Supporting Information

ABSTRACT: Superconcentrated "water-in-salt" electrolytes have greatly widened the electrochemical stable window (ESW) of aqueous electrolytes, but they also generate new problems, including high costs, high viscosity, and low conductivity. Here we report a 2 m low concentration electrolyte using an *N*,*N*-dimethylformamide/water (DMF/H_2O) hybrid solvent, which provides a wider ESW (2.89 V) than an aqueous electrolyte (2.66 V) and presents nonflammability, high conductivity, and low viscosity characteristics. In 2 m DMF/H_2O hybrid electrolyte, the LUMO energy of the DMF solvent (−0.00931 a.u.) is lower than that of H_2O (−0.00735 a.u.), which could effectively promote the degradation of FSI^- and lead to stable solid electrolyte interphase formation. As a result, the electrochemical reversibility and cyclability of the $KTi_2(PO_4)_3$@C (KTP@C) anode in the aqueous electrolyte have been significantly enhanced with the help of DMF addition. Moreover, the $K_2Zn_3(Fe(CN)_6)_2$ (KZnHCF)//KTP@C full potassium-ion battery exhibits highly efficient stability and rate capability with a long cycle performance over 10 000 cycles and delivers a specific discharge capacity of 33 mAh g^{-1} at a high current density of 20 A g^{-1}. Low concentrations of DMF/H_2O hybrid electrolytes can inhibit the hydrogen evolution reaction of aqueous electrolytes, providing more opportunities for the practical application of electrode materials. Not limited to DMF solvent, mixing organic and aqueous solvents will provide more available options and perspectives for improving the energy density and long cycle performance of the aqueous metal-ion battery.

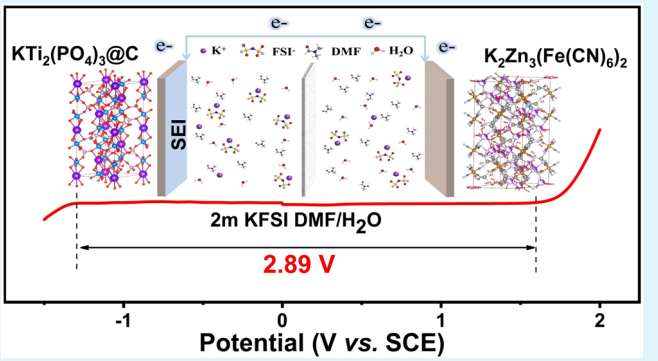

KEYWORDS: *DMF, SEI, low concentration, hybrid electrolyte, aqueous potassium-ion batteries, wide electrochemical window*

INTRODUCTION

The rapid consumption of nonrenewable energy has attracted the attention of both academia and industry; expanding the utilization of renewable wind, solar, and geothermal energy has become a global trend.[1] However, renewable energies are prone to be intermittent and unpredictable in nature. Therefore, it is very important to develop efficient, convenient, and green energy storage technology.[2,3] Rechargeable batteries, especially lithium-ion batteries (LIBs), have received much more attention among all electrochemical energy storage systems. However, the safety risks of commercial LIBs still exist on account of their flammable organic solvent and unstable lithium salt of $LiPF_6$. An aqueous metal-ion battery, a promising candidate for grid energy storage, delivers highly safe features, low cost, and high ionic conductivity.[4−6] However, the electrochemical stable window (ESW) (1.23 V) of pure H_2O restrains the choice of cathode and anode materials for battery devices and limits the energy density of aqueous metal-ion battery devices.[5,7,8]

In the past few years, "water-in-salt" electrolytes,[9−12] "water-in-bisalt" electrolytes,[13,14] and hydrate-melt electrolytes[15,16] effectively expanded the ESW by reducing the number of free H_2O molecules and changing the structure of the solvent sheath. Although increasing the concentration of electrolytes can increase the ESW of electrolytes to some extent, the highly concentrated electrolytes still generate new issues, including high cost, low ion diffusion rate, and ionic conductivity characteristics of aqueous electrolytes caused by the rapid rise of electrolyte viscosity.[7] Actually, when the salt concentration of the electrolyte increases to a certain value, the ESW of the electrolyte no longer expands significantly. Given that the salt concentration of the electrolyte ranges from 21 to 28 m, the ESW on the anode side only increases by 0.1 V.[13] Therefore, low viscosity and high ionic conductivity of aqueous electrolyte are key parameters for achieving the high electrochemical performance of aqueous devices. In addition to increasing the salt

Received: May 5, 2021
Accepted: July 26, 2021

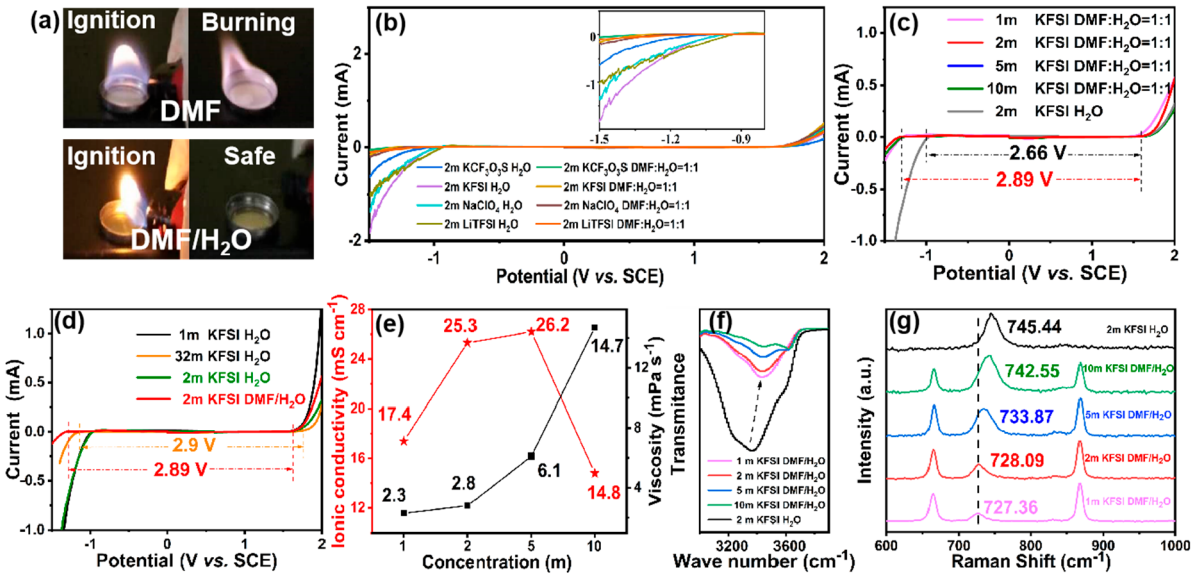

Figure 1. Physicochemical properties of DMF/H_2O hybrid electrolytes. (a) The flammability of the solvent when ignited using a lighter: pure DMF (top) and DMF/H_2O (bottom). (b) ESW of various electrolytes. (c) ESW of DMF/H_2O hybrid electrolyte at different concentrations. (d) ESW of KFSI in an aqueous electrolyte and a DMF/H_2O hybrid electrolyte. (e, f, g) Conductivity and viscosity, FTIR, and Raman spectra of KFSI in a DMF/H_2O hybrid electrolyte at different concentrations.

concentration, the design of solvents presents new opportunities. A series of new electrolytes produced by mixing aqueous and nonaqueous solvents have been reported. Wang et al.[17] dissolved LiTFSI in a mixture of H_2O and DMC, which could change the solvation structure of the aqueous electrolyte and lead to the formation of an additional mesophase (alkylcarbonate) on the electrode surface. In addition, good SEI formation could benefit from the suppression effect of HER. Dou et al.[18] reported an "acetonitrile/water in salt" (AWIS) hybrid electrolyte, which delivered nonflammability and a wide ESW of 3.0 V and further remarkably enhanced the ionic conductivity and decreased the viscosity of the hybrid electrolyte. The 5 m AWIS electrolyte facilitated supercapacitor devices to achieve long cycling stability over 14 000 cycles with a high operating voltage of 2.2 V. Recently, Xie et al.[19] designed a 2 m low concentration "molecular crowding electrolyte" by mixing water-miscible poly(ethylene glycol) (94% PEG) into H_2O, which exhibited a high ESW of 3.2 V and extremely low ionic conductivity (0.8 mS cm^{-1}) of 2 m LiTFSI−94%PEG−6% H_2O electrolyte. Therefore, it is necessary to consider how to reduce the salt concentration as far as possible without sacrificing the ionic conductivity.

Here, we introduce a universal aqueous/nonaqueous hybrid electrolyte based on *N,N*-dimethylformamide/water (DMF/H_2O), achieving a wide ESW (2.89 V) with relatively low concentration (2 m), high conductivity, and low viscosity. The DMF solvent promotes the degradation of FSI^- in the electrolyte, leading to protective SEI formation of $-CF_x$ and KF on the anode surface. The 2 m KFSI DMF/H_2O hybrid electrolyte enables an available discharge capacity for KTP@C in the potassium-ion battery (PIB), which cannot operate due to its low redox potential in general aqueous electrolytes. The aqueous KZnHCF//KTP@C full battery exhibits good rate performance and stable cycling performance over 10 000 cycles.

RESULTS AND DISCUSSION

A series of low concentration electrolytes were obtained by dissolving different salts of lithium, sodium, and potassium (LiTFSI, $NaClO_4$, KFSI, and KCF_3O_3S) in *N,N*-dimethylformamide/water (DMF/H_2O) mixed solvent. DMF solvent is selected as a cosolvent owing to its strong polarity and good miscibility with H_2O solvent.[20] The mixed solvent was prepared by mixing DMF and H_2O at different molar ratios (2:1, 1:1, 1:2), and the flammability is shown in Figure 1a and Figure S1. Pure DMF solvent exhibits highly flammable characterization (digital photo at the top of Figure 1a), while optimized mixed solvent (the molar ratio of DMF: H_2O is 1:1) delivers a nonflammable feature (digital photo at the bottom of Figure 1a and Figure S1). Linear sweep voltammetry (LSV) tests were applied to determine the ESW of various electrolytes, in which the Pt electrode serves as both working and counter electrodes and the saturated calomel electrode (SCE) works as a reference electrode. Onset potential is defined as the corresponding electrochemical potential when the current density is 0.5 mA cm^{-2}. In Figure 1b, the ESW of 2 m DMF/H_2O hybrid electrolytes is higher than that of the 2 m aqueous electrolyte. Compared with highly concentrated electrolytes, low concentration electrolytes are expected to offer lower viscosity and higher conductivity.[7,9,18] Among 2 m hybrid electrolytes with different salts, the KFSI-based electrolytes exhibit the highest conductivity (25.3 mS cm^{-1}) and the lowest viscosity (2.8 mPa s^{-1}, Figure S2). As shown in Figure 1c, KFSI-based hybrid electrolytes of all concentrations deliver a wide ESW of 2.89 V. Specifically, the ESW of the 2 m KFSI DMF/H_2O hybrid electrolyte (2.89 V, −1.29 to 1.60 V vs. SCE) is higher than that of the 2 m KFSI aqueous electrolyte (2.66 V, −1.04 to 1.62 V vs. SCE), indicating that DMF cosolvent has an essential role in expanding the ESW of aqueous electrolytes, especially in the HER direction. Although a 32 m KFSI aqueous electrolyte also provides a wide ESW of 2.9 V (Figure 1d), the hybrid electrolytes achieve comparable ESW with a substantially lower concentration. The conductivity and viscosity of electro-

https://doi.org/10.1021/acsami.1c08151
ACS Appl. Mater. Interfaces XXXX, XXX, XXX−XXX

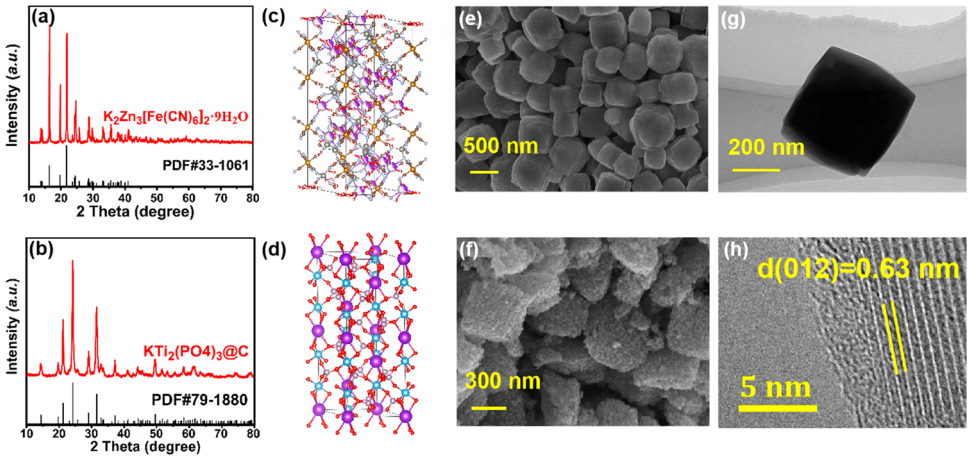

Figure 2. Structure characterization of the as-prepared KZnHCF and KTP@C samples. (a, c, e, g) XRD, crystal structure, SEM, and TEM images of KZnHCF, respectively. (b, d, f, h) XRD, crystal structure, SEM, and TEM images of KTP@C, respectively.

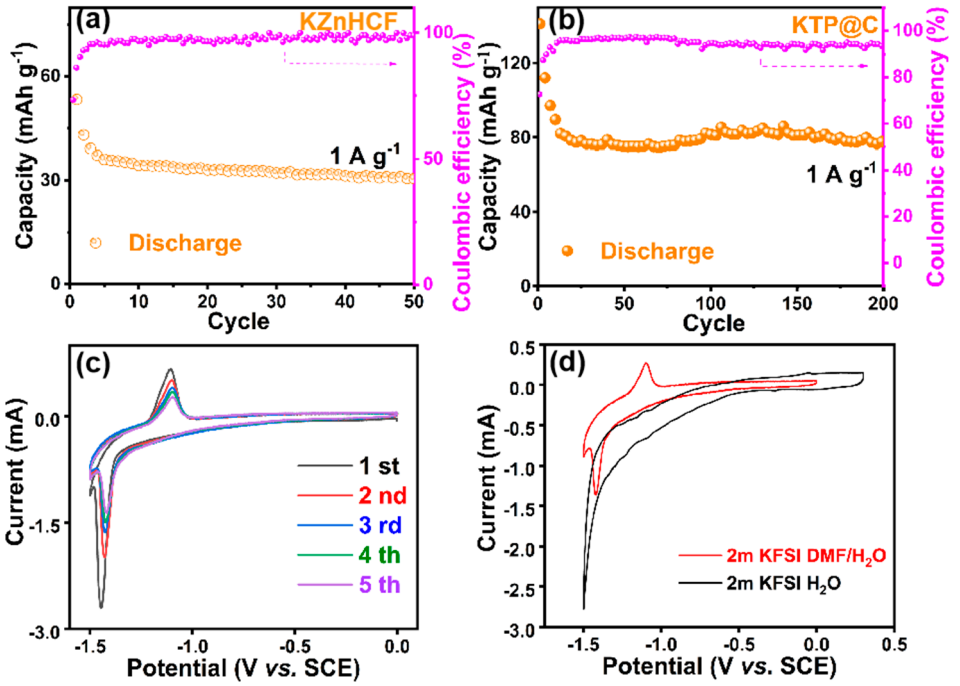

Figure 3. Electrochemical performance of KZnHCF and KTP@C electrodes. (a, b) Cycling performance of the KZnHCF cathode and KTP@C anode in 2 m KFSI DMF/H_2O electrolyte at 1 A g^{-1}, respectively. (c) The CV curves of KTP@C in 2 m KFSI DMF/H_2O electrolyte between −1.5 and 0 V vs SCE at a scan rate of 0.5 mV s^{-1}. (d) CV curves comparison of KTP@C in 2 m KFSI DMF/H_2O and 2 m KFSI aqueous electrolytes.

lytes with 1, 2, 5, and 10 m KFSI in DMF/H_2O were measured, and the viscosity of the electrolyte increases as the concentration increases (Figure 1e). The conductivity reaches its maximum value at a concentration of 5 m and then decreases because the strong coordination between the anions and cations will reduce the conductivity of the electrolyte when the concentration reaches a certain value.[18] Overall, the 2 m KFSI DMF/H_2O hybrid electrolyte not only inherits the high ESW (~2.89 V) of the high concentration electrolyte but also presents the low viscosity (2.8 mPa s^{-1}) and conductivity (25.3 mS cm^{-1}) of the low concentration electrolyte. FTIR and Raman spectroscopy were recorded to have a better understanding of the molecular structure of the DMF/H_2O hybrid electrolyte. In Figure 1f, a peak at 3000−3700 cm^{-1} in the aqueous electrolyte is assigned to O−H stretching of free H_2O molecules, indicating that free H_2O molecules gather to form an extensive network of intermolecular hydrogen bonding. When DMF is added, the intensity of the O−H stretching in H_2O decreases significantly, indicating that the hydrogen-bonding network is broken in the entire solution system.[12] In Figure 1g, the S−N−S stretching modes of FSI^- in different electrolytes have been revealed via Raman spectra. Comparing the state of the 2 m KFSI aqueous electrolyte, the S−N−S (FSI^-) vibration in the DMF/H_2O hybrid electrolyte experiences a red shift from 745.44 to 728.09 cm^{-1}. It is believed that adding organic solvent weakens the interaction between anions and cations.[18] In addition, in a DMF/H_2O hybrid electrolyte with a high concentration of 5 m, the interaction between anions and cations strengthens gradually and causes the decrease of conductivity and the increase of viscosity. Therefore, a low concentration DMF/H_2O hybrid electrolyte can effectively expand the ESW by

https://doi.org/10.1021/acsami.1c08151
ACS Appl. Mater. Interfaces XXXX, XXX, XXX−XXX

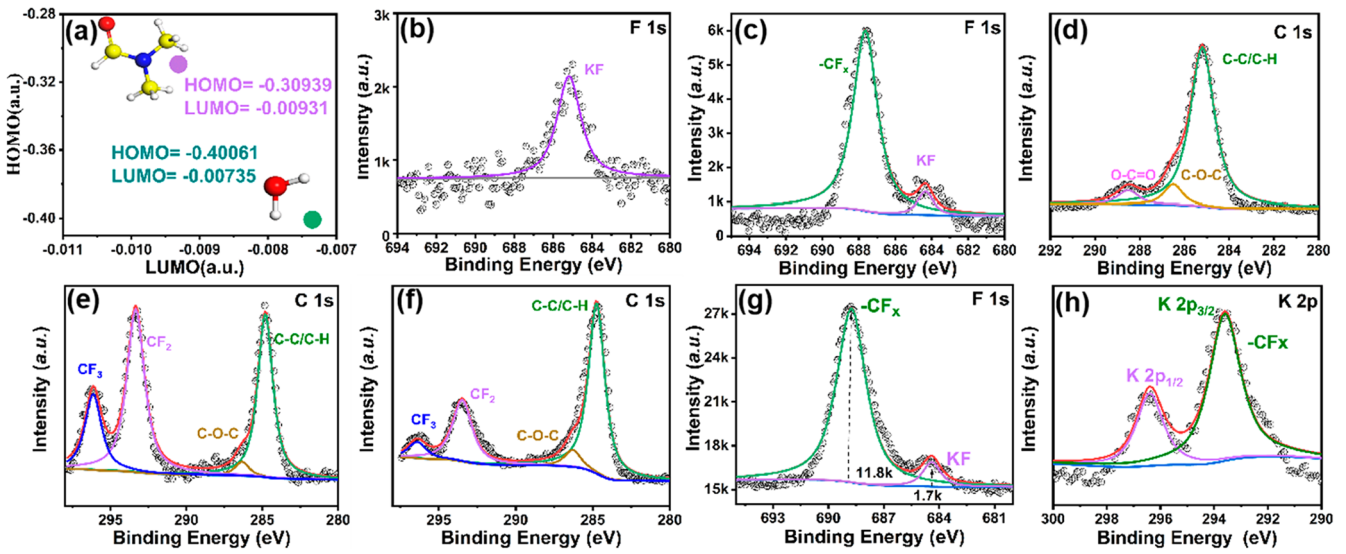

Figure 4. SEI characterization. (a) HOMO/LUMO energies (a.u.) of DMF and H_2O. The ex situ XPS spectra of Ti foil F 1s in the (b) 2 m KFSI aqueous electrolyte and (c) 2 m KFSI DMF/H_2O electrolyte and C 1s in the (d) DMF/H_2O solvent and (e) 2 m KFSI DMF/H_2O electrolyte. The ex situ XPS spectra of KTP (f) C 1s, (g) F 1s, and (h) K 2p after 1000 cycles of the full cells at 1 A g^{-1} in 2 m KFSI DMF/H_2O hybrid electrolyte.

significantly inhibiting the HER at the anode side and enable more electrode materials for aqueous battery devices.

Compared with aqueous LIBs, aqueous PIBs have some merits owing to abundant resources, high ionic conductivity, and similar physical and chemical properties to aqueous LIBs.[21−23] Very few anode materials are currently available for aqueous PIBs due to the large ionic radius of potassium, which causes significant volume change in the anode during the K^+ insertion/extraction. In addition, only some materials with open frameworks (superionic conductors and metal−organic frameworks) that could work at a relatively high potential are suitable for aqueous PIBs. Among the candidates for anode materials, superion conductor (NASICON) $KTi_2(PO_4)_3$ can be considered to be promising due to its open three-dimensional structure.[24,25] Ji et al. first used $KTi_2(PO_4)_3$ as an anode material for aqueous PIBs with a high concentration electrolyte of potassium acetate (30 m KAc), which delivered a discharge capacity of 35 mAh g^{-1} after 500 cycles and 40 mAh g^{-1} after 11 000 cycles at 1 A g^{-1}.[26] However, $KTi_2(PO_4)_3$ has not been used in a low concentration aqueous electrolyte because its narrow ESW causes HER at the K^+ storage potential of the $KTi_2(PO_4)_3$, as previously observed in 1 and 10 m KAc electrolytes.[26] Here, KTP@C material[35] was synthesized by a hydrothermal method with a follow-up heat treatment and used as the anode. $K_2Zn_3[Fe(CN)_6]_2{\cdot}9H_2O$ (KZnHCF), a Prussian blue analogue,[27,28] was used as the cathode material, and 2 m KFSI DMF/H_2O hybrid electrolyte was used as the electrolyte. The X-ray diffraction (XRD) patterns (Figures 2a and 2b) closely fit the standard diffraction patterns of KZnHCF (JCPDS No. 33-1061) and KTP@C (JCPDS No. 79-1880). The crystal structures of KZnHCF and KTP@C are shown in Figure 2c and 2d, respectively. The scanning electron microscope (SEM) image and transmission electron microscope (TEM) image in Figures 2e and 2f show nanocubes of cathode and anode materials with sizes ranging from 500 to 700 nm. The TEM image (Figure 2g) of KTP@C demonstrates nanocubes with an edge length of 600−700 nm. The *d*-spacing of 0.63 nm observed (Figure 2h) could be attributed to the (012) crystal plane of KTP@C. The large interstitial space of the 3D framework enables the rapid diffusion of K^+ in KZnHCF and KTP@C materials.

The electrochemical performance of KTP@C and KZnHCF electrodes was further studied in three-electrode cells. KZnHCF, as a cathode material, delivers a stable specific capacity of 32 mAh g^{-1} at a current of 1 A g^{-1} after 50 cycles in 2 m KFSI DMF/H_2O hybrid electrolyte (Figure 3a, the theoretical capacity of KZnHCF is 62.8 mAh g^{-1}). In Figure 3b, the KTP@C anode exhibits good cycling stability with a specific capacity of 76 mAh g^{-1} at 1 A g^{-1} after 200 cycles in 2 m KFSI DMF/H_2O hybrid electrolyte. The irreversible loss of capacity during discharging is owing to the reduction of FSI^- and the decomposition of H_2O.[29] Note that the decomposition of H_2O in this system does not sacrifice electrolyte safety (Figure S3 and Movies S1−S4). The CV curves of the KTP@C anode and KZnHCF cathode (Figure 3c and Figure S4a) are consistent with the voltage−capacity profiles (Figures S4b and S5), showing redox couples at −1.1/-1.4 and 0.8/1.1 V vs SCE. In the 2 m KFSI aqueous electrolyte, there is no significant redox peak in the CV curve of the KTP@C anode (Figure 3d), which is totally different from the result in the 2 m KFSI DMF/H_2O hybrid electrolyte. Therefore, benefitting from DMF, a low concentration 2 m KFSI DMF/H_2O hybrid electrolyte enables the practical application of KTP@C material.

To further understand how the electrolyte expands the HER potential threshold of ESW and improves the specific capacity of the electrode materials, the Gaussian 09 package was used to calculate the HOMO/LUMO energies of the hybrid electrolyte system (computational details are listed in the Supporting Information).[30] In Figure 4a, the LUMO energy of DMF (−0.00931 a.u.) is more negative than that of H_2O (−0.00735 a.u.), indicating that DMF has a preference for the electron reduction process over H_2O molecules. To figure out the SEI formation mechanism, the LSV tests were conducted in a three-electrode system (Ti foil as the working electrode) between −1.5 and 0 V at a scan rate of 0.5 mV s^{-1}. The products deposited on the Ti foil were analyzed through X-ray photoelectron spectroscopy (XPS). Figures 4b and 4c demonstrate the F 1s spectra from samples tested in 2 m KFSI

https://doi.org/10.1021/acsami.1c08151
ACS Appl. Mater. Interfaces XXXX, XXX, XXX−XXX

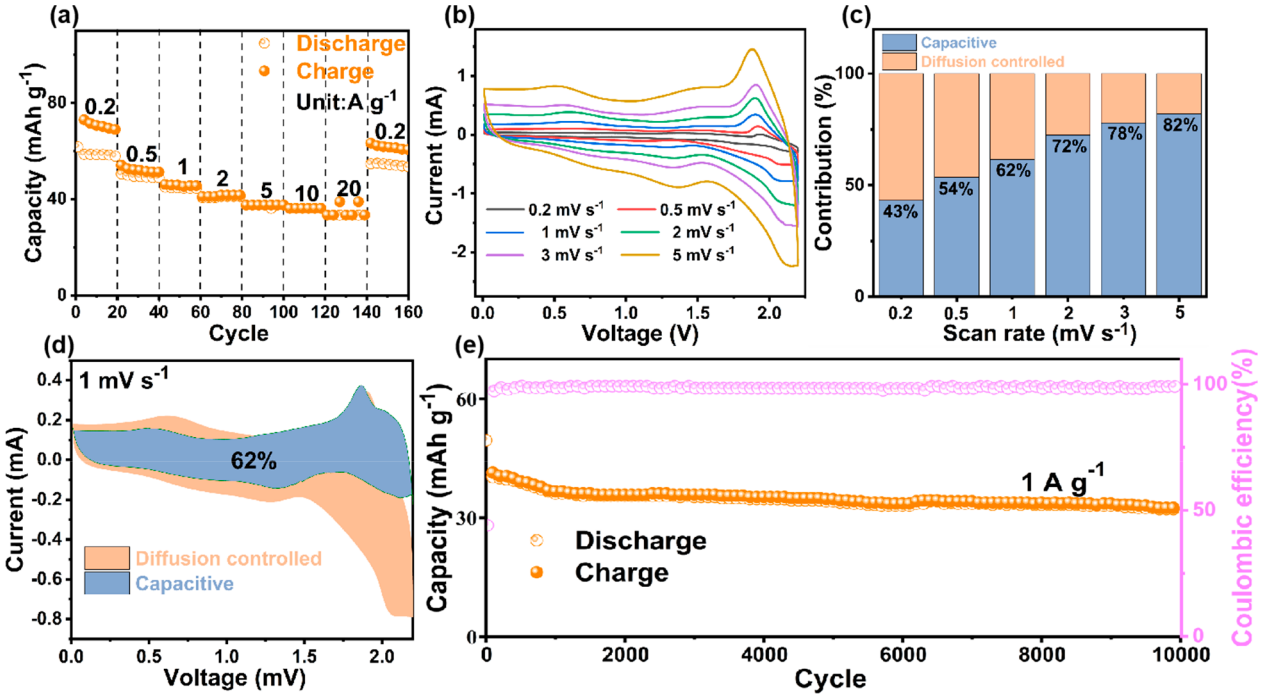

Figure 5. Electrochemical performance of the KZnHCF//2 m KFSI DMF/H_2O//KTP@C full battery. (a) Rate capability at various current densities. (b) The CV curves of the KZnHCF//2 m KFSI DMF/H_2O//KTP@C full battery between 0 and 2.2 V at multiple scan rates from 0.2 to 5 mV s^{-1}. (c) Capacitive contribution ratios at different scan rates. (d) Capacity contribution curves at 1 mV s^{-1}. (e) Long term cycling performance of the KZnHCF//2 m KFSI DMF/H_2O//KTP@C full battery at 1 A g^{-1}.

aqueous and 2 m KFSI DMF/H_2O electrolytes, respectively. One peak at 685.18 eV can be identified in the F 1s spectra from the sample tested in the 2 m KFSI aqueous electrolyte, and it could correspond to KF in the SEI film. Interestingly, in the SEI of the sample tested in the 2 m KFSI DMF/H_2O electrolyte, a new strong peak ($-CF_x$) appears at 687.64 eV, indicating that DMF could promote the degradation of FSI^- and result in the formation of $-CF_x$ and KF, which eventually accumulate into a protective SEI film.[31] At the same time, the C 1s spectra from samples tested in the DMF/H_2O solvent and 2 m KFSI DMF/H_2O hybrid electrolyte are shown in Figures 4d and 4e, respectively. In DMF/H_2O solvent, the three peaks at 284.8, 286.1, and 288.1 eV in the C 1s spectra are assigned to C−C/C═H, C−O−C, and O−C═O bonds, respectively. In 2 m KFSI DMF/H_2O hybrid electrolyte, the C−O−C and O−C═O peaks become weaker and even disappear while new peaks ($-CF_3$, $-CF_2$) appear at 293.3 and 296.1 eV, which are consistent with F 1s spectra. This result suggests that at least part of the $-CF_x$ came from DMF, confirming that DMF participates in the formation of SEI. To verify the results from the electrochemically inert Ti foil, we performed an XPS test on the KTP electrode of the full cell after 1000 cycles at 1 A g^{-1} in 2 m KFSI DMF/H_2O hybrid electrolyte. There is no carbon coated on the KTP electrode, so the effect from carbon can be excluded. The results are similar to those on Ti foil and also demonstrate strong $-CF_x$ signals, as seen in Figures 4f and 4g. In addition, the existence of the KF species suggests that the S−F bond in the FSI^- has been completely broken. Figure 4h demonstrates the K $2p_{1/2}$ at 293.6 eV and K $2p_{3/2}$ and $-CF_x$ at 296.4 eV (signals of the K $2p_{3/2}$ and $-CF_x$ group overlap).[32] Therefore, the component of the SEI layer mainly contains $-CF_x$ groups, KF, sulfur oxide species, and carbonate species (Figure S6). An EIS test was also used to study the interfacial behaviors with a three-electrode system. As shown in Figure S7a, the KTP@C electrode consists of one semicircle (charge-transfer resistance) before and after 50 cycles in 2 m KFSI aqueous solution; the semicircle represents the charge-transfer resistance of the interface between KTP@C and the electrolyte. The charge-transfer resistance increases after 50 cycles, indicating the instability of interfacial behaviors in 2 m KFSI aqueous electrolyte. By contrast, in Figure S7b, the KTP@C electrode in 2 m KFSI DMF/H_2O consists of two semicircles before and after cycling. The spontaneous SEI on the surface of the KTP@C electrode appears as the first semicircle in the high frequency range in the 2 m KFSI DMF/H_2O hybrid electrolyte.[33] Specifically, a stable interface ($-CF_x$ groups, KF, sulfur oxide species, and carbonate species were confirmed in XPS results, as shown in Figure 4) remains on the surface of the KTP@C electrode after the electrolyte immersed and the cell cycled. The charge transfer across the SEI is responsible for the semicircle in the low frequency range. The almost constant impedance before and after 50 cycles indicates the stability of the interface, which is more conducive to enhancing the electrochemical performance of aqueous battery devices.

A KZnHCF//KTP@C full PIB was assembled to evaluate the 2 m KFSI DMF/H_2O hybrid electrolyte. The active mass of KZnHCF is excessive, and the active mass ratio between KZnHCF and KTP@C is about 2:1. At current densities of 0.2, 0.5, 1, 2, 5, and 10 A g^{-1}, the KZnHCF//KTP@C full battery delivers a discharge capacity of 57, 49, 44, 41, 37, and 36 mAh g^{-1} and then recovers to 54 mAh g^{-1} at 0.2 A g^{-1}. The high capacity of 33 mAh g^{-1} even at a high current density of 20 A g^{-1} corresponds to the charge and discharge rate of 156 C (Figure 5a). To figure out the electrochemical kinetics during the charge and discharge process, the ratio of diffusion-controlled and capacitive contribution has been ensured through CV at different scan rates from 0.2 to 5 mV s^{-1} (Figure 5b). Similar shapes of CV curves can be observed at different scan rates, but

https://doi.org/10.1021/acsami.1c08151
ACS Appl. Mater. Interfaces XXXX, XXX, XXX−XXX

the slight peak shifts are ascribed to the contribution of capacitive behavior in the cathodic and anodic peaks. In order to analyze this behavior, the following eq 1[34,35] is used for analysis:

$$i\,(\mathrm{V}) = k_1 v + k_2 v^{1/2} \quad (1)$$

which can be converted to

$$i\,(\mathrm{V})/v^{1/2} = k_1 v^{1/2} + k_2 \quad (2)$$

where v, i, $k_1 v$, and $k_2 v^{1/2}$ represent scan rate, current, and contributions of capacitive and diffusion-controlled behavior, respectively. The values of k_1 and k_2 can be quantified as the contributions of capacitive and diffusion-controlled behaviors. The capacitive contributions at different scan rates are shown in Figures 5c and 5d, which exhibit the contribution ratios of 43%, 54%, 62%, 72%, 78%, and 82% at the scan rates of 0.2, 0.5, 1.0, 2.0, 3.0, and 5.0 mV s^{-1}, respectively. Thus, the capacitive-controlled charge will be dominant at high rates, demonstrating that capacitive charge storage has a significant impact on capacity. Figure S8 demonstrates the galvanostatic charge and discharge curves of KZnHCF//KTP@C full PIB at 1 A g^{-1} in different cycles. The KZnHCF//KTP@C full PIB delivers a stable reversible capacity of 38 mAh g^{-1} after 200 cycles at 0.2 A g^{-1} (Figure S9) and 32 mAh g^{-1} after 10 000 cycles at 1 A g^{-1}, which may be partly attributed to stable electrode materials and interfaces in the hybrid electrolyte (Figure 5e).

CONCLUSION

In conclusion, we have developed a variety of DMF/H_2O hybrid electrolytes (LiTFSI, $NaClO_4$, KFSI, and KCF_3O_3S) with wide ESW, nonflammability, low viscosity, and high conductivity features. The 2 m KFSI DMF/H_2O hybrid electrolyte (ESW of 2.89 V) significantly boosts the electrochemical reversibility of KTP@C (KTP@C electrode cannot operate in the aqueous electrolyte), and KTP@C achieves a specific capacity of 76 mAh g^{-1} at 1 A g^{-1} after 200 cycles. The improvement of the electrochemical performance of the KTP@C electrode should be attributed to the DMF solvent that can effectively promote the degradation of FSI^- and participate in a stable SEI formation. The KZnHCF//KTP@C full PIB delivers a long cycle stability over 10 000 cycles and exhibits a specific capacity of 33 mAh g^{-1} at a high rate of 20 A g^{-1}. The low concentration DMF/H_2O electrolyte with a more negative HER potential enables the application of aqueous anode materials, which supports potential development for low cost, durable energy storage devices.

EXPERIMENTAL SECTION

Anode Materials. The $KTi_2(PO4)_3$@C (KTP@C) anode material was synthesized by a hydrothermal method and carbon-coating treatment. The synthesis method can be referred to in a previous work.[35]

Cathode Material. The $K_2Zn_3[Fe(CN)_6]_2{\cdot}9H_2O$ (KZnHCF) cathode material was synthesized by a citrate-assisted coprecipitation method.[36] A mixed solution was made up of $ZnSO_4$ (0.01 mol L^{-1}) and potassium citrate (0.15 mol L^{-1}) dissolved in 100 mL of H_2O, and then 100 mL of 0.01 mol L^{-1} $K_4Fe(CN)_6{\cdot}3H_2O$ was added into solution A. After stirring for 24 h at room temperature, the precipitate from the mixed solution was obtained through filtration and washed several times. Finally, the precipitate was dried at 110 °C overnight in a vacuum to obtain KZnHCF samples.

Electrolytes. Preparation of DMF/H_2O hybrid electrolytes: the mixed solvent was prepared by mixing DMF and H_2O in molar ratios of 1:1 or other values (2:1, 1:2), and a corresponding stoichiometric amount of metal salt was added into the mixed solvent to form hybrid electrolytes with different concentrations (2 m LITFSI (0.574 g) in DMF/H_2O (1 g, 1:1), 2 m $KOSO_2CF_3$ (0.376 g) in DMF/H_2O (1 g, 1:1), 2 m $NaClO_4$ (0.245 g) in DMF/H_2O (1 g, 1:1), 1, 2, 5, and 10 m KFSI (0.219, 0.438, 1.095, and 2.192 g) in DMF/H_2O (1 g, 1:1)). The control electrolyte was 2 m KFSI (0.438 g) dissolved in pure water (1 g).

Material Characterization. The crystal structure of materials was identified by X-ray diffraction (XRD, Bruker D8 Advance diffractometer) with Cu Kα radiation (λ = 1.5405 Å). The morphologies and microstructural characterizations of the materials were obtained by scanning electron microscopy (SEM, ZEISS Supra 55) and transmission electron microscopy (TEM, Tecnai G2F20s-Twin). Surface components of materials were analyzed by X-ray photoelectron spectroscopies (XPS, Thermo Fisher ESCALAB 250Xi).

Electrolyte Characterization. The ionic conductivity of various electrolytes was recorded by an electrical conductivity meter DDS-307 (INESA Scientific Instrument Co., Ltd.). The viscosity of the electrolytes was tested by a rotational rheometer Haake MARS III (Thermo Fisher Scientific). The flammability of the electrolyte was tested via igniting the presoaked glass fibers separators in the electrolyte. Linear sweep voltammetry (LSV) profiles were used to measure the ESW at 10 mV s^{-1} using 2 mm platinum disc as both working and counter electrodes and a saturated calomel electrode (SCE) as a reference electrode. Raman spectra were obtained using a Lab Ram HR Evolution Series High-Resolution Raman Spectrometer (HORIBA Jobin Yvon SAS). Fourier transform infrared (FTIR) spectra were measured using a Nicolet iS50.

Electrochemical Characterization. The KTP@C anode, KZnHCF cathode, and active carbon (YP50) auxiliary electrodes were fabricated by mixing the active material, conductive material (Ketjenblack), and binder (poly(tetrafluoroethylene), PTFE) at a mass ratio of 7:2:1. Then the electrode materials were dried at 110 °C for 12 h in a vacuum drying oven, and the mass of the electrode was weighed and the electrode pressed on a Ti mesh. In three-electrode battery measurements, electrode materials served as the working electrode, YP50 as the counter electrode, and SCE as the reference electrode, respectively. Cyclic voltammetry (CV) and LSV were applied using a CHI600E electrochemical workstation. The full PIBs were assembled in CR2032 coin cells using a KTP@C cathode, KZnHCF anode, glass fiber (Whatman GF/A) as the separator, and 2 m KFSI DMF/H_2O as the electrolyte, respectively. The cutoff voltage range of the full PIB cell was 0.01−2.2 V.

ASSOCIATED CONTENT

Supporting Information

The Supporting Information is available free of charge at https://pubs.acs.org/doi/10.1021/acsami.1c08151.

Flammability test, conductivity and viscosity tests, CV curves, charge−discharge curves, XPS, and EIS profile (PDF)

Flammability test of the glass fiber (Whatman GF/A) of the KZnHCF//KTP@C full battery between 0 and 2.2 V at 1 A g^{-1} in 2 m KFSI DMF after 3 cycles (MP4)

Flammability test in 2 m KFSI DMF/H_2O after 3 cycles (MP4)

Flammability test after 100 cycles (MP4)

Flammability test after 350 cycles (MP4)

AUTHOR INFORMATION

Corresponding Author

Rui Li − *School of Advanced Materials, Peking University Shenzhen Graduate School, Shenzhen 518055, China;* orcid.org/0000-0001-5480-8089; Email: liruisz@pku.edu.cn

https://doi.org/10.1021/acsami.1c08151
ACS Appl. Mater. Interfaces XXXX, XXX, XXX−XXX

Authors

Xinran Yuan − *School of Advanced Materials, Peking University Shenzhen Graduate School, Shenzhen 518055, China*

Yibo Li − *School of Advanced Materials, Peking University Shenzhen Graduate School, Shenzhen 518055, China*

Yanan Zhu − *School of Advanced Materials, Peking University Shenzhen Graduate School, Shenzhen 518055, China*

Wenjun Deng − *School of Advanced Materials, Peking University Shenzhen Graduate School, Shenzhen 518055, China*

Chang Li − *School of Advanced Materials, Peking University Shenzhen Graduate School, Shenzhen 518055, China*

Zhuqing Zhou − *School of Advanced Materials, Peking University Shenzhen Graduate School, Shenzhen 518055, China*

Jun Hu − *School of Advanced Materials, Peking University Shenzhen Graduate School, Shenzhen 518055, China*

Man Zhang − *School of Advanced Materials, Peking University Shenzhen Graduate School, Shenzhen 518055, China*

Haibiao Chen − *School of Advanced Materials, Peking University Shenzhen Graduate School, Shenzhen 518055, China*

Complete contact information is available at: https://pubs.acs.org/10.1021/acsami.1c08151

Notes

The authors declare no competing financial interest.

■ ACKNOWLEDGMENTS

This work was supported by the Shenzhen Science and Technology Innovation Commission (JCYJ20180504165506495).

■ REFERENCES

(1) Sharma, S. S.; Manthiram, A. Towards More Environmentally and Socially Responsible Batteries. *Energy Environ. Sci.* **2020**, *13*, 4087−4097.

(2) Dunn, B.; Kamath, H.; Tarascon, J. M. Electrical Energy Storage for the Grid: A Battery of Choices. *Science* **2011**, *334*, 928−935.

(3) Goodenough, J. B. Electrochemical Energy Storage in a Sustainable Modern Society. *Energy Environ. Sci.* **2014**, *7* (1), 14−18.

(4) Huang, J.; Guo, Z.; Ma, Y.; Bin, D.; Wang, Y.; Xia, Y. Recent Progress of Rechargeable Batteries Using Mild Aqueous Electrolytes. *Small Methods* **2019**, *3*, 1800272.

(5) Kim, H.; Hong, J.; Park, K. Y.; Kim, H.; Kim, S. W.; Kang, K. Aqueous Rechargeable Li and Na Ion Batteries. *Chem. Rev.* **2014**, *114* (23), 11788−827.

(6) Liu, Z.; Huang, Y.; Huang, Y.; Yang, Q.; Li, X.; Huang, Z.; Zhi, C. Voltage Issue of Aqueous Rechargeable Metal-Ion Batteries. *Chem. Soc. Rev.* **2020**, *49* (1), 180−232.

(7) Chao, D.; Qiao, S. Toward High-Voltage Aqueous Batteries: Super- or Low-Concentrated Electrolyte. *Joule* **2020**, *4*, 1846−1851.

(8) Huang, S.; Zhu, J.; Tian, J.; Niu, Z. Recent Progress in the Electrolytes of Aqueous Zinc-Ion Batteries. *Chem. - Eur. J.* **2019**, *25* (64), 14480−14494.

(9) Suo, L.; Borodin, O.; Gao, T.; Olguin, M.; Ho, J.; Fan, X.; Luo, C.; Wang, C.; Xu, K. Water in-Salt" Electrolyte Enables High-Voltage Aqueous Lithium-ion Chemistries. *Science* **2015**, *350*, 938−943.

(10) Sun, W.; Suo, L.; Wang, F.; Eidson, N.; Yang, C.; Han, F.; Ma, Z.; Gao, T.; Zhu, M.; Wang, C. Water-in-Salt" Electrolyte Enabled $LiMn_2O_4/TiS_2$ Lithium-Ion Batteries. *Electrochem. Commun.* **2017**, *82*, 71−74.

(11) Jiang, L.; Lu, Y.; Zhao, C.; Liu, L.; Zhang, J.; Zhang, Q.; Shen, X.; Zhao, J.; Yu, X.; Li, H.; Huang, X.; Chen, L.; Hu, Y. Building Aqueous K-Ion Batteries for Energy Storage. *Nat. Energy* **2019**, *4* (6), 495−503.

(12) Chen, L.; Zhang, J.; Li, Q.; Vatamanu, J.; Ji, X.; Pollard, T. P.; Cui, C.; Hou, S.; Chen, J.; Yang, C.; Ma, L.; Ding, M.; Garaga, M.; Greenbaum, S.; Lee, H.-S.; Borodin, O.; Xu, K.; Wang, C. A 63m Superconcentrated Aqueous Electrolyte for High-Energy Li-Ion Batteries. *ACS Energy Lett.* **2020**, *5*, 968−974.

(13) Suo, L.; Borodin, O.; Sun, W.; Fan, X.; Yang, C.; Wang, F.; Gao, T.; Ma, Z.; Schroeder, M.; von Cresce, A.; Russell, S. M.; Armand, M.; Angell, A.; Xu, K.; Wang, C. Advanced High-Voltage Aqueous Lithium-Ion Battery Enabled by "Water-in-Bisalt" Electrolyte. *Angew. Chem., Int. Ed.* **2016**, *55*, 7136−7141.

(14) Ko, S.; Yamada, Y.; Yamada, A. A 62 m K-Ion Aqueous Electrolyte. *Electrochem. Commun.* **2020**, *116*, 106764.

(15) Yamada, Y.; Usui, K.; Sodeyama, K.; Ko, S.; Tateyama, Y.; Yamada, A. Hydrate-Melt Electrolytes for High-Energy-Density Aqueous Batteries. *Nat. Energy* **2016**, *1*, 16129.

(16) Miyazaki, K.; Takenaka, N.; Watanabe, E.; Iizuka, S.; Yamada, Y.; Tateyama, Y.; Yamada, A. First-Principles Study on the Peculiar Water Environment in a Hydrate-Melt Electrolyte. *J. Phys. Chem. Lett.* **2019**, *10*, 6301−6305.

(17) Wang, F.; Borodin, O.; Ding, M. S.; Gobet, M.; Vatamanu, J.; Fan, X.; Gao, T.; Eidson, N.; Liang, Y.; Sun, W.; Greenbaum, S.; Xu, K.; Wang, C. Hybrid Aqueous/Non-aqueous Electrolyte for Safe and High-Energy Li-Ion Batteries. *Joule* **2018**, *2* (5), 927−937.

(18) Dou, Q.; Lei, S.; Wang, D.-W.; Zhang, Q.; Xiao, D.; Guo, H.; Wang, A.; Yang, H.; Li, Y.; Shi, S.; Yan, X. Safe and High-Rate Supercapacitors Based on an "Acetonitrile/Water in Salt" Hybrid Electrolyte. *Energy Environ. Sci.* **2018**, *11*, 3212−3219.

(19) Xie, J.; Liang, Z.; Lu, Y. Molecular Crowding Electrolytes for High-Voltage Aqueous Batteries. *Nat. Mater.* **2020**, *19*, 1006−1011.

(20) Zhang, X.; Zhao, D.; Zhao, Y.; Tang, P.; Shen, Y.; Xu, C.; Li, H.; Xiao, Y. High Performance Asymmetric Supercapacitor Based on MnO_2 Electrode in Ionic Liquid Electrolyte. *J. Mater. Chem. A* **2013**, *1* (11), 3706−3712.

(21) Kim, H.; Kim, J. C.; Bianchini, M.; Seo, D.-H.; Rodriguez-Garcia, J.; Ceder, G. Recent Progress and Perspective in Electrode Materials for K-Ion Batteries. *Adv. Energy Mater.* **2018**, *8* (9), 1702384.

(22) Zhang, W.; Liu, Y.; Guo, Z. Approaching High-Performance Potassium-Ion Batteries *via* Advanced Design Strategies and Engineering. *Sci. Adv.* **2019**, *5*, 7412.

(23) Rajagopalan, R.; Tang, Y.; Ji, X.; Jia, C.; Wang, H. Advancements and Challenges in Potassium Ion Batteries: A Comprehensive Review. *Adv. Funct. Mater.* **2020**, *30* (12), 1909486.

(24) Zhang, R.; Huang, J.; Deng, W.; Bao, J.; Pan, Y.; Huang, S.; Sun, C. Safe, Low-Cost, Fast-Kinetics and Low-Strain Inorganic-Open-Framework Anode for Potassium-Ion Batteries. *Angew. Chem., Int. Ed.* **2019**, *58* (46), 16474−16479.

(25) Han, J.; Niu, Y.; Bao, S. J.; Yu, Y. N.; Lu, S. Y.; Xu, M. Nanocubic $KTi_2(PO_4)_3$ Electrodes for Potassium-Ion Batteries. *Chem. Commun.* **2016**, *52* (78), 11661−11664.

(26) Leonard, D. P.; Wei, Z.; Chen, G.; Du, F.; Ji, X. Water-in-Salt Electrolyte for Potassium-Ion Batteries. *ACS Energy Lett.* **2018**, *3* (2), 373−374.

(27) Islas-Vargas, C.; Guevara-García, A.; Oliver-Tolentino, M.; Ramos-Sánchez, G.; González, I.; Galván, M. Experimental and Theoretical Investigation on the Origin of the High Intercalation Voltage of $K_2Zn_3[Fe(CN)_6]_2$ Cathode. *J. Electrochem. Soc.* **2019**, *166*, 5139−5145.

(28) Lu, Y.; Wang, L.; Cheng, J.; Goodenough, J. B. Prussian Blue: a New Framework of Electrode Materials for Sodium Batteries. *Chem. Commun.* **2012**, *48* (52), 6544−6546.

(29) Suo, L.; Oh, D.; Lin, Y.; Zhuo, Z.; Borodin, O.; Gao, T.; Wang, F.; Kushima, A.; Wang, Z.; Kim, H. C.; Qi, Y.; Yang, W.; Pan, F.; Li, J.; Xu, K.; Wang, C. How Solid-Electrolyte Interphase Forms in Aqueous Electrolytes. *J. Am. Chem. Soc.* **2017**, *139*, 18670−18680.

(30) You, L.; Duan, K.; Zhang, G.; Song, W.; Yang, T.; Song, X.; Wang, S.; Liu, J. *N,N*-Dimethylformamide Electrolyte Additive Via a Blocking Strategy Enables High-Performance Lithium-Ion Battery under High Temperature. *J. Phys. Chem. C* **2019**, *123* (10), 5942−5950.

(31) Wang, Z.; Qi, F.; Yin, L.; Shi, Y.; Sun, C.; An, B.; Cheng, H.; Li, F. An Anion-Tuned Solid Electrolyte Interphase with Fast Ion. *Adv. Energy Mater.* **2020**, *10*, 1903843.
(32) Ren, X.; He, M.; Xiao, N.; McCulloch, W. D.; Wu, Y. Greatly Enhanced Anode Stability in K-Oxygen Batteries with an In Situ Formed Solvent- and Oxygen-Impermeable Protection Layer. *Adv. Energy Mater.* **2017**, *7* (1), 1601080.
(33) Guo, W.; Zhang, W.; Si, Y.; Wang, D.; Fu, Y.; Manthiram, A. Artificial Dual Solid-Electrolyte Interfaces Based on *in situ* Organothiol Transformation in Lithium Sulfur Battery. *Nat. Commun.* **2021**, *12*, 3031.
(34) Wang, J.; Polleux, J.; Lim, J.; Dunn, B. Pseudocapacitive Contributions to Electrochemical Energy Storage in TiO_2 (Anatase) Nanoparticles. *J. Phys. Chem. C* **2007**, *111*, 14925−14931.
(35) Li, Y.; Deng, W.; Zhou, Z.; Li, C.; Zhang, M.; Yuan, X.; Hu, J.; Chen, H.; Li, R. An Ultra-Long Life Aqueous Full K-Ion Battery. *J. Mater. Chem. A* **2021**, *9*, 2822−2829.
(36) Deng, W.; Li, Z.; Ye, Y.; Zhou, Z.; Li, Y.; Zhang, M.; Yuan, X.; Hu, J.; Zhao, W.; Huang, Z.; Li, C.; Chen, H.; Zheng, J.; Li, R. Zn^{2+} Induced Phase Transformation of $K_2MnFe(CN)_6$ Boosts Highly Stable Zinc-Ion Storage. *Adv. Energy Mater.* **2021**, 202003639.

https://doi.org/10.1021/acsami.1c08151
ACS Appl. Mater. Interfaces XXXX, XXX, XXX−XXX